JmlID 109_ArtID 1799_Proof# 1 - 18/05/2019

Journal of Molecular Medicine
https://doi.org/10.1007/s00109-019-01799-5

JMolMed

ORIGINAL ARTICLE

The median eminence as the hypothalamic area involved in rapid transfer of glucose to the brain: functional and cellular mechanisms

Fernando Martínez[1,2,3] · Manuel Cifuentes[4] · Juan Carlos Tapia[5] · Francisco Nualart[1,2,3]

Received: 20 January 2019 / Revised: 3 May 2019 / Accepted: 13 May 2019

Abstract

Our data proposes that glucose is transferred directly to the cerebrospinal fluid (CSF) of the hypothalamic ventricular cavity through a rapid "fast-track-type mechanism" that would efficiently stimulate the glucosensing areas. This mechanism would occur at the level of the median eminence (ME), a periventricular hypothalamic zone with no blood-brain barrier. This "fast-track" mechanism would involve specific glial cells of the ME known as β2 tanycytes that could function as "inverted enterocytes," expressing low-affinity glucose transporters GLUT2 and GLUT6 in order to rapidly transfer glucose to the CSF. Due to the large size of tanycytes, the presence of a high concentration of mitochondria and the expression of low-affinity glucose transporters, it would be expected that these cells accumulate glucose in the endoplasmic reticulum (ER) by sequestering glucose-6-phosphate (G-6-P), in a similar way to that recently demonstrated in astrocytes. Glucose could diffuse through the cells by micrometric distances to be released in the apical region of β2 tanycytes, towards the CSF. Through this mechanism, levels of glucose would increase inside the hypothalamus, stimulating glucosensing mechanisms quickly and efficiently.

Key messages

- Glucose diffuses through the median eminence cells (β2 tanycytes), towards the hypothalamic CSF.
- Glucose is transferred through a rapid "fast-track-type mechanism" via GLUT2 and GLUT6.
- Through this mechanism, hypothalamic glucose levels increase, stimulating glucosensing.

Keywords Tanycytes · GLUT2 · GLUT6 · Median eminence · Glucose sensing · Brain · Barrier

Introduction

The hypothalamus is one of the primary centers involved in the control of food intake [1]. Located in the basal region of the third ventricle, the hypothalamus contains neuronal and glial populations that respond to changes in glucose concentrations [2–5]. This structure contacts the cerebrospinal fluid (CSF) through tanycytes, specialized ependymal-glial cells. There are four subpopulations of tanycytes: α1, α2, β1, and β2. β1 tanycytes express the glucose transporter, GLUT2, in

Electronic supplementary material The online version of this article (https://doi.org/10.1007/s00109-019-01799-5) contains supplementary material, which is available to authorized users.

✉ Fernando Martínez
femartin@udec.cl

✉ Francisco Nualart
frnualart@udec.cl

[1] Laboratory of Neurobiology and Stem Cells, NeuroCellT, Department of Cellular Biology, Faculty of Biological Sciences, University of Concepcion, Concepcion, Chile

[2] Center for Advanced Microscopy CMA BIO BIO, University of Concepcion, Concepcion, Chile

[3] Departamento de Biología Celular, Facultad de Ciencias Biológicas, Universidad de Concepción, Casilla 160-C, Concepción, Chile

[4] Department of Cell Biology, Genetics and Physiology, IBIMA, BIONAND, Andalusian Center for Nanomedicine and Biotechnology and Networking Research Center on Bioengineering, Biomaterials and Nanomedicine, University of Malaga, Malaga, Spain

[5] Facultad de Ciencias de la Salud, Universidad de Talca, Talca, Chile

JmlID 109_ArtID 1799_Proof# 1 - 18/05/2019

the apical region, as well as other proteins involved in the peripheral glucose-sensing mechanism, such as glucokinase (GK) and the potassium channel subunit, kir 6.1 [6–10]. Recently, studies of hypothalamic sections and primary cultures have shown that β1 tanycytes respond to changes in glucose concentrations with increased intracellular calcium [4, 5, 11]. We believe that the hypothalamic brain parenchyma is not exposed to high concentrations of glucose. Under conditions of hyperglycemia, when glucose can reach 25 mM in the plasma, glucose concentration in the hypothalamus varies by no more than 1 or 2 mM, reaching total concentrations in the tissue of nearly 3 mM [12, 13]. Conversely, the glucose concentration in the CSF varies proportionally with that in the bloodstream [14–16]. Because the glucosensing regions in the brain are situated near the brain ventricles, rapid variations in glucose concentrations in the CSF allow the ventricles to detect changes in the systemic glucose [10].

It has long been postulated that glucose uptake by the CSF is produced through the choroid plexus, a circumventricular organ. However, the choroid plexus has a limited capacity for incorporating glucose because (i) the greatest concentration of the glucose transporter, GLUT1, occurs in the basolateral region of the cell, in the vascular area [17, 18] and (ii) the glucose transporter, GLUT1, is saturated at vascular glucose concentrations > 8 mM, which would not allow an efficient transfer of glucose to the CSF at vascular concentrations > 10 mM. The median eminence (ME), another circumventricular organ located in the basal region of the third ventricle, contains the primary plexus of the hypophyseal portal system, which allows the transfer of hormones from the hypothalamus to the anterior pituitary [19, 20]. This primary plexus consists of fenestrated blood vessels without a blood-brain barrier, thereby allowing the direct exchange of metabolites between the blood and the ME parenchyma. At this level, diffusion of polar molecules, such as glucose, is limited by the cerebral barrier between the ME and the CSF. This barrier consists of tight junctions from β2 tanycytes that form the floor of the third ventricle [19, 21–24]. For glucose to enter the CSF of the third ventricle, there must be specific transport systems in β2 tanycytes that allow the concentration of glucose at this level.

In mammals, the process of glucose uptake by cells is performed through the concentrating transport systems known as sodium-glucose transporters (SGLTs) [25] and the facilitative transporters of hexose GLUTs [26, 27]. The latter are responsible for non-concentrated and saturated glucose uptake so that some members of this family of transporters are involved in the transfer of glucose from the blood to nervous tissue [28]. The isoforms of hexose GLUT transporters mainly expressed in the brain are GLUT1 and GLUT3 [28–32]. To a lesser extent, GLUT2 and GLUT4 have been located [6, 33–35], as have the last cloned isoforms GLUT6 and GLUT8 [36, 37]. Because the GLUT2 isoform has a Michaelis constant of 15–20 mM [38], its participation has been proposed in the trans-epithelial glucose transport mechanism from the diet in the small intestine. Since the isoform has a high transport capacity and is located on both the apical and basolateral faces [39], it is presented as a model that can be analogous to the situation of glucose transport from the blood into the CSF through the ME during hyperglycemia. Moreover, the expression of GLUT6 in systems of membranes reconstituted from COS-7 cells shows glucose transport activity at high substrate concentrations. Furthermore, studies of binding to cytochalasin B revealed that, like GLUT2, GLUT6 has a low affinity for this substrate, suggesting that it has a low affinity for glucose transport [40]. Based on the characteristics of these isoforms, it seems relevant to analyze the location of these transporters, both of which have low affinity for glucose transport in the β2 tanycytes of ME.

In this context, it is feasible to postulate that β2 tanycytes transport glucose transcellularly from the EM portal capillaries to the CSF of the infundibular recess, using the functional expression of GLUT2 and GLUT6.

Results

Hyperglycemia does not change the normal cellular structure of the ME but increases Evans blue diffusion between the hypothalamic ME and ventricular CSF

The basal third ventricle and the hypothalamic infundibular recess (Fig. 1a) is a particular cavity surrounded by polarized α and β tanycytes. Most tanycytes have blebs in the apical membrane, which have normal morphology in hyperglycemia (Fig. 1a$_1$–a$_3$). The ME is formed for β2 tanycytes, which form the blood-EM-CSF barrier (Figure 1a and a$_4$). We used trypan blue intravascular injection to observe that normoglycemia and hyperglycemia do not change the general histological properties of the ME vascular area and tanycyte distribution (Fig. 1b–f). In hyperglycemic condition, trypan blue was observed normally distributed in the ME blood vessels and surrounding brain tissue (Fig. 1e and f). No staining was detected inside the ventricular cavity (Fig. 1). Additionally, β2 tanycytes showed a normal distribution in the ME, and were positive for vimentin (Fig. 1g and i) and were efficiently transduced with the adenovirus Ad-GFP (Fig. 1h, inset and i). We also defined that GFAP-positive astrocytes were normally observed in hypothalamic tissue and ME (Fig. 1h) and have a differential distribution than Ad-GFP-positive tanycytes (Fig. 1h, inset). The portal blood vessels (hypothalamic-hypophyseal portal system) showed a normal distribution with fenestrated capillaries in different regions of the median eminence (Fig. 1j–l, arrowheads).

To analyze the blood-EM-CSF barrier functional activity, we detected Evans blue in normo- and hyperglycemic

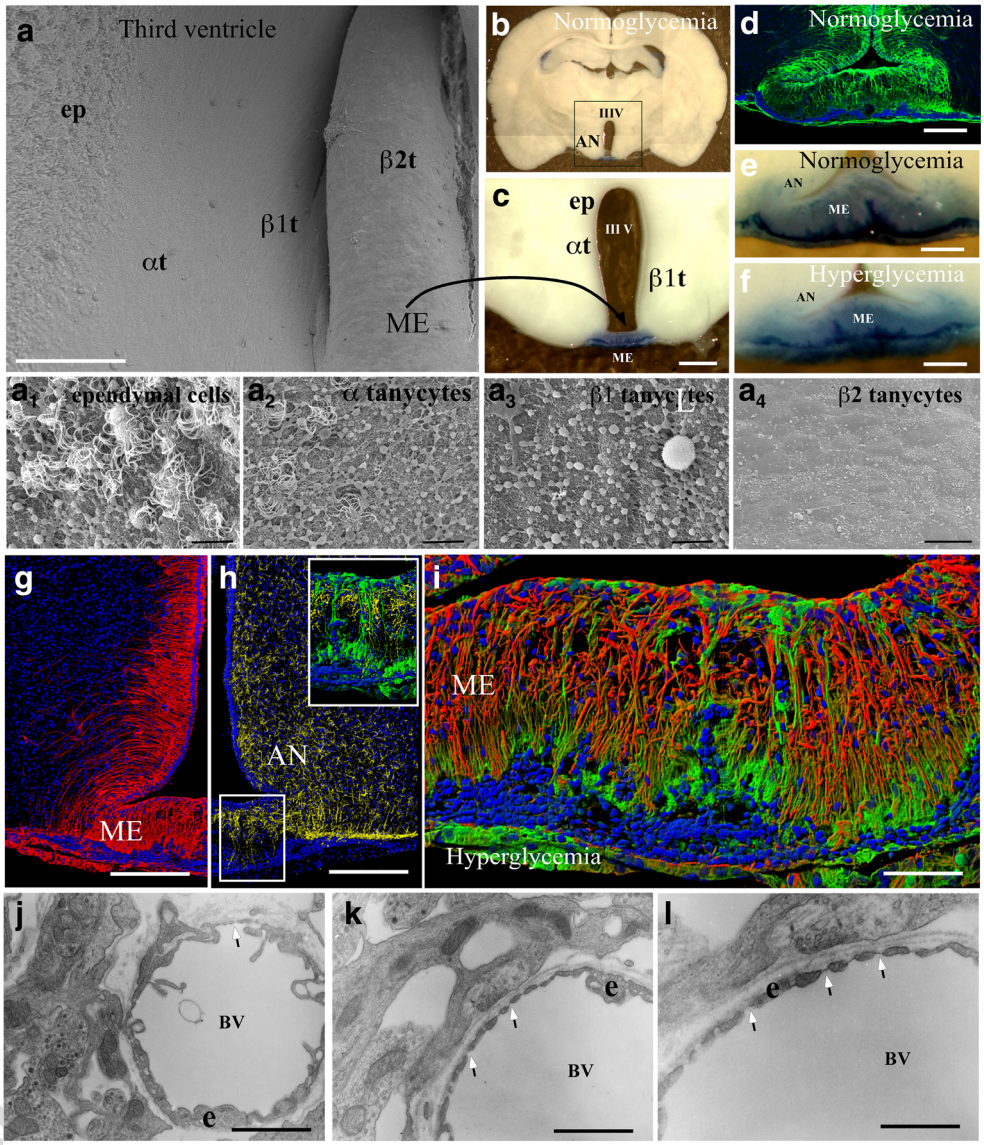

Blood vessels, median eminence

Fig. 1 Structural analysis of the hypothalamic median eminence in hyperglycemic condition. **a** Scanning electron microscopy of the mediobasal hypothalamus, detecting α and β tanycytes (**a1**–**a4**). **b**–**f** Alcian blue vascular injection in normo- and hyperglycemic conditions to define the blood-ME barrier. **g**–**I** Confocal microscopy analysis of tanycytes and astrocytes distribution. The cells were identified using anti-vimentin (**g**, red), anti-GFAP (**h**, yellow), or using adenovirus-GFP injected inside the CSF (**h**, inset). **i** Median eminence injected with adenovirus-GFP and immunostained with anti-vimentin. Tile- and Z-stack scanning using rendering analysis with Imaris Software. Hoechst was used for nuclear staining (blue). **j**–**l** TEM analysis of the ME blood vessels; palisade region. IIIV, third ventricle; AN, arcuate nucleus; ep, ependymal cells; e, endothelial cells; ME, median eminence; BV, blood vessel. Scale bars: **a**–**f**, **g**–**h**, 150 μm; **a1**–**a4**, 20 μm; **i**, 50 μm; **j**, 5 μm; **k**, 3 μm; **l**, 1 μm. All images are representative of different biologically independent samples. 1**a**–**d**, $n = 6$. **e**–**f**, $n = 3$. **g**–**I**, $n = 6$. **j**–**L**, $n = 3$

conditions (Fig. 2). In normoglycemia, Evans blue was detected in the rostral portal plexus vessels and ME milieu but not in β1 tanycytes inside the rostral ventricle (Fig. 2a–e), which were identified with anti-vimentin (Fig. 2e-merge). Astrocytes were also detected using anti-GFAP (red cells). In hyperglycemia, Evans blue was detected in the ME milieu and inside β2 tanycytes (Fig. 2f–j). Surprisingly, Evans blue was also detected in α and β1 tanycytes inside the third ventricle (Fig. 2i–j). Only the tanycytes (vimentin-positive, J and merge) were positive for Evans blue. The astrocytes (GFAP-positive, J and merge) distributed inside the hypothalamus were Evans blue-negative. Similar results were observed in the caudal hypothalamic region (Fig. 2k–n and insets); increased Evans blue labeling was observed inside the ME and hypothalamic tanycytes. Finally, we observed that Evans blue was detected in the ME milieu and also inside β2 tanycytes (green cells), but not inside the astrocytes (red cells) in both normoglycemia (Fig. 2o–r) and hyperglycemia (Fig. 2s–v). At the subcellular level, similar results were obtained in β1 and α tanycytes in hyperglycemia (Fig. 2 j and j-merge). These results suggest that hyperglycemia resulted in Evans blue transfer from the ME to the hypothalamic third ventricle walls. Additionally, most of the Evans blue was detected intracellularly in both β2 and β1 tanycytes.

β2 tanycytes induce sub-cellular changes in the end-feet processes that contact the fenestrated blood vessels in hyperglycemia

We analyzed the structural cellular modification in β2 tanycytes under hyperglycemia in 40-μm sections by immunohistochemical analysis using anti-vimentin (Fig. 3a–c). β2

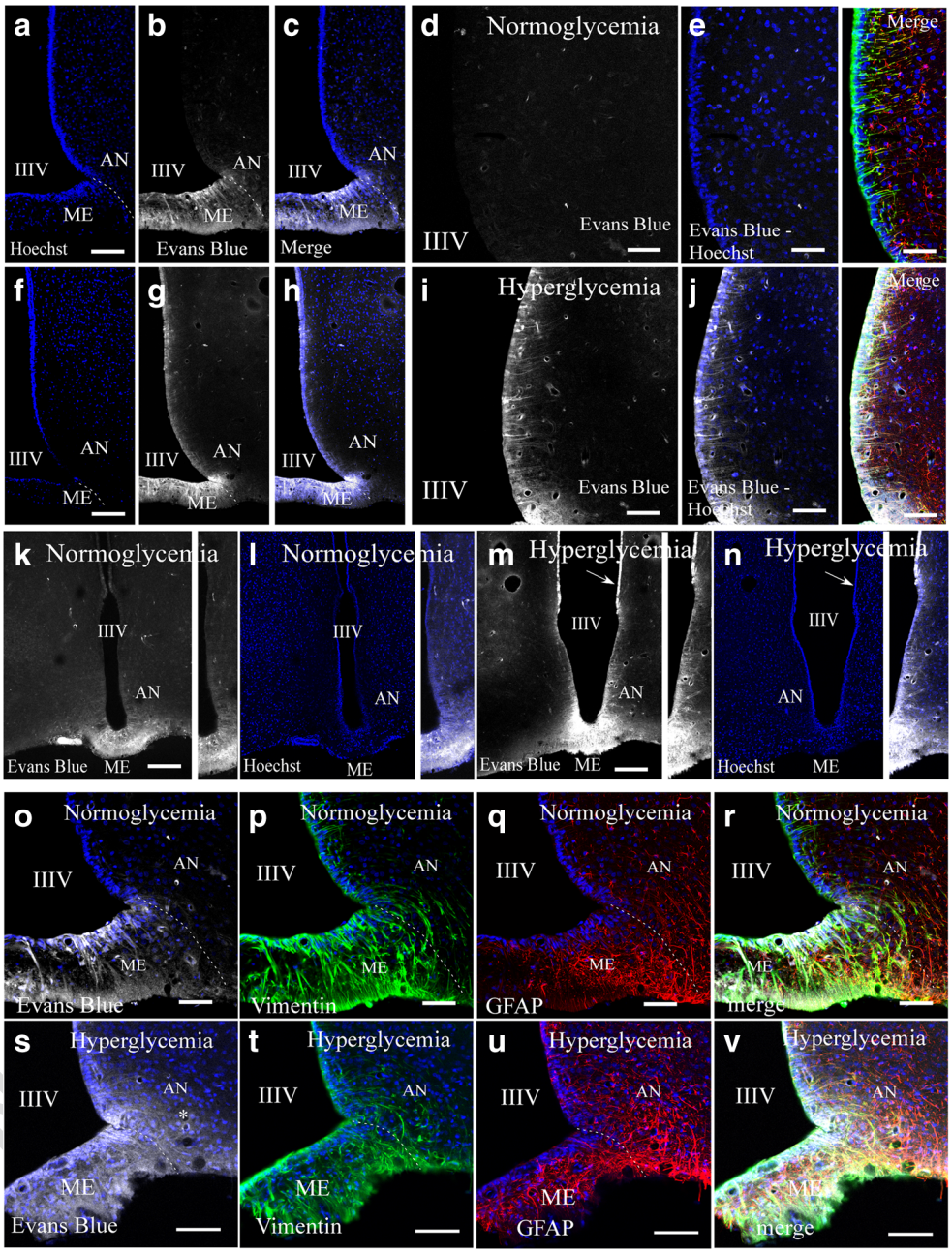

Fig. 2 Increased distribution of Evans blue throughout tanycytes in the median eminence in hyperglycemia. **a**–**E** Frontal section of the rostral hypothalamus after vascular Evans blue injection in normoglycemic condition. Immunohistochemical analysis with anti-vimentin (merge, green) or anti-GFAP (merge, red). **f**–**j** Frontal section of the rostral hypothalamus after vascular Evans blue injection in hyperglycemic condition. Analysis of the hypothalamic tanycytes (arrows). Immunohistochemical analysis with anti-vimentin (merge, green) or anti-GFAP (merge, red). **k**–**n** Frontal section of the posterior hypothalamus after vascular Evans blue injection in normoglycemic (**k** and **l**) or hyperglycemic (**m** and **n**) conditions. Tanycytes and ependymal cells (arrows). **o**–**v** Evans blue cellular distribution in the median eminence tanycytes in normoglycemic (**o**–**r**) or hypoglycemic (**s**–**v**) conditions. Immunohistochemical analysis with anti-vimentin (green) or anti-GFAP (red). IIIV, third ventricle; AN, arcuate nucleus; ME, median eminence. Scale bars: **a**–**n**, 50 μm; **o**–**v**, 30 μm. All images are representative of different biologically independent samples. **a**–**e**, $n = 6$. **f**–**j**, $n = 6$. **o**–**r**; **s**–**v**, $n = 6$

tanycytes increased process branching that forms the previously defined "palisade area" contacting portal blood vessels (Fig. 3c, arrows). Similar results were obtained by immunohistochemical analysis using floating thin sections (50 μm) comparing normoglycemic and hyperglycemic conditions with Z-stack confocal analysis. Hyperglycemia induces cellular changes only in β2 tanycytes (palisade area, arrows), but not in astrocytes (blue-light cells) (Fig. 3e–g) located mainly in the ventricular area of the ME (arrows). The same results were observed in animals with normoglycemic or hyperglycemic conditions analyzed with confocal microscopy, Z-stack analysis and renderization imaging (Fig. 3h, i). In the palisade region, cellular branching in hyperglycemia was apparent. β2 tanycyte branching contacted the portal vessels (Fig. 3g_1, g_2, and G_3), which were not observed in normoglycemia (Fig. 3e_1, e_2, e_3). Additionally, we used serial 1-μm semi-thin sections to define the blood vessels inside the ME ventricular area (Fig. 3j, area i) or the ME palisade area (Fig. 3j, area II) in normoglycemia and hyperglycemia. Quantitative analysis showed increased portal blood vessel area inside the palisade region but not in the ventricular area in hyperglycemic conditions (Fig. 3l and m). Ultrastructural analysis showed a normal distribution of β2 tanycytes and blood vessels in normoglycemia; however, in hyperglycemia, β2 tanycytes

exhibited an irregular interaction between the end-processes and the perivascular area of portal vessels. A dilated perivascular space was detected (Fig. 3t, green area) and dilated inter-cellular spaces were also observed between β2 tanycyte end-processes (Fig 3t, asterisks) and around the β2 tanycyte processes inside the ME (Fig. 3v). These processes were enlarged (Image V) to compare them with the cellular processes observed in normoglycemia (Image U). In the apical part of the ME (periventricular area), high cellular interdigitation and normal pericellular spaces were observed in normo- and hyperglycemic samples (Fig. 3x, y). Additionally, a small number of cells displayed short microvilli (Fig. 3y).

To analyze tight junction structural modifications, we analyzed serial ultrathin sections (50 nm) using a high concentration of osmium tetroxide covering 1 μm of the samples. No structural alteration in the tight junction formation was detected in any of the sections analyzed, indicating that the ME-CSF barrier was not altered (Fig. 3z_1–z_4, arrow). Additionally, we observed that a large number of cells lost their basal projections, maintaining their insertion in the epithelial barrier (Fig. 3z, large arrows). This was not a problem of sectioning because the eventual process was not observed in the ultrastructural 3D reconstruction of the tissue area. Finally, some cells showed a large amount of ER and some mitochondria in the cytosol when they acquired this "balloon-like" form (Fig. 3z_3).

Finally, we observed three different areas of the hypothalamus to define regional-specific structural changes in β2 tanycytes under hyperglycemia. We determined that the anterior region of the ME shows the greatest structural changes in the tanycytes (Supplementary Fig. 1a, d versus b, e and c, f). This region is the one that receives the main blood influx and is the area most exposed to hyperglycemia. Additionally, the normal tanycyte structure was recovered with a return to normoglycemia (Supplementary Fig. 1g, h, i). These results show that the structural changes in tanycytes are dynamic and respond to vascular glucose levels.

GLUT2 and GLUT6 are expressed in hypothalamic β2 tanycytes under normo- and hyperglycemia conditions with GLUT2 mainly polarized to the end-feet vascular processes and GLUT6 mostly intracellular

The low-affinity transporters, GLUT2 and GLUT6, have been poorly studied in the central nervous system. GLUT2 has been linked to the glucose-sensing system because it is present in the glial cells of the hypothalamus and some ependymal cells. However, the distribution of GLUT2 and GLUT6 in the glial cells involved in barriers, such as β2 tanycytes, is completely unknown. Non-isotopic in situ hybridization analysis confirmed GLUT2 and GLUT6 mRNA expression in β2 tanycytes with most of the positive reaction located in the ventricular area of the cells (Fig. 4a–b). However, GLUT2 mRNA was also detected in the Palisade region of the ME around the portal vessels (Fig. 4a, arrowheads). The expression of these transporters was also observed using RT-PCR and qRT-PCR analyses after laser microdissection (LMD) (Fig. 4e–g). A similar concentration of GLUT2 was detected in the ME, arcuate nucleus (AN), and ependymal cells (Ep) (Fig. 4h). Only ependymal cells showed increased GLUT2 expression. Similarly, GLUT6 mRNA concentration was observed in both the ME and AN. Ependymal cells also showed a higher expression of GLUT6 (Fig. 4h).

Next, we used immunohistochemical analysis to define GLUT2 and GLUT6 distribution in rat ME. In normoglycemia, GLUT2 and GLUT6 were detected with low immunoreaction in β2 tanycytes (Fig. 4i–k and o–k); however, we observed a positive signal in β1 tanycytes (Fig. 4j, arrow). In hyperglycemia, both GLUT2 and GLUT6 were detected with higher immunoreaction. GLUT2 was mainly detected in the Palisade area (Fig. 4l–m, arrows), and GLUT6 was present in different regions of β2 tanycytes (ventricular, intermedia, and Palisade area) (Fig. 4r–t, arrows) with a vesicular and reticular pattern of immunoreaction (Fig. 4s, arrowheads). Small cells with high GLUT6 immunoreaction were also detected in the ME-CSF barrier (Fig. 4s, asterisks).

In hyperglycemia, glucose concentrations in the ventricular CSF (glycorrhachia) decreases under GLUT2 and GLUT6 inhibition

A functional relationship between the CSF of the third ventricle and the cerebral glucose-sensing system has not been established to date. The ventricular walls of the basal hypothalamus do not contain cilia (Fig. 1a). Therefore, the movement of the CSF is very slow, generating hydrodynamic conditions that are favorable for sensing a metabolite like glucose. Obtaining CSF from the third ventral ventricle is technically complex, but we have standardized this procedure by installing permanent intra-cerebral cannulas before obtaining any samples or performing the experiment. In this work, cannulas were installed through stereotactic surgery in the lateral ventricle and third ventricle (basal) of the hypothalamus, and the proportional transfer of glucose was analyzed in both compartments of CSF after peripherally increasing the glucose concentration (controlled hyperglycemia of 25 mM). We have standardized the methodology for establishing normoglycemia (5 mM glucose) or hyperglycemia (25 mM glucose) with a single intraperitoneal injection of glucose. The glucose concentration is measured after obtaining CSF from each cannula through efflux at different times after achieving hyperglycemia. Only one 2-μL sample of CSF is needed to establish the measurements. When inducing hyperglycemia,

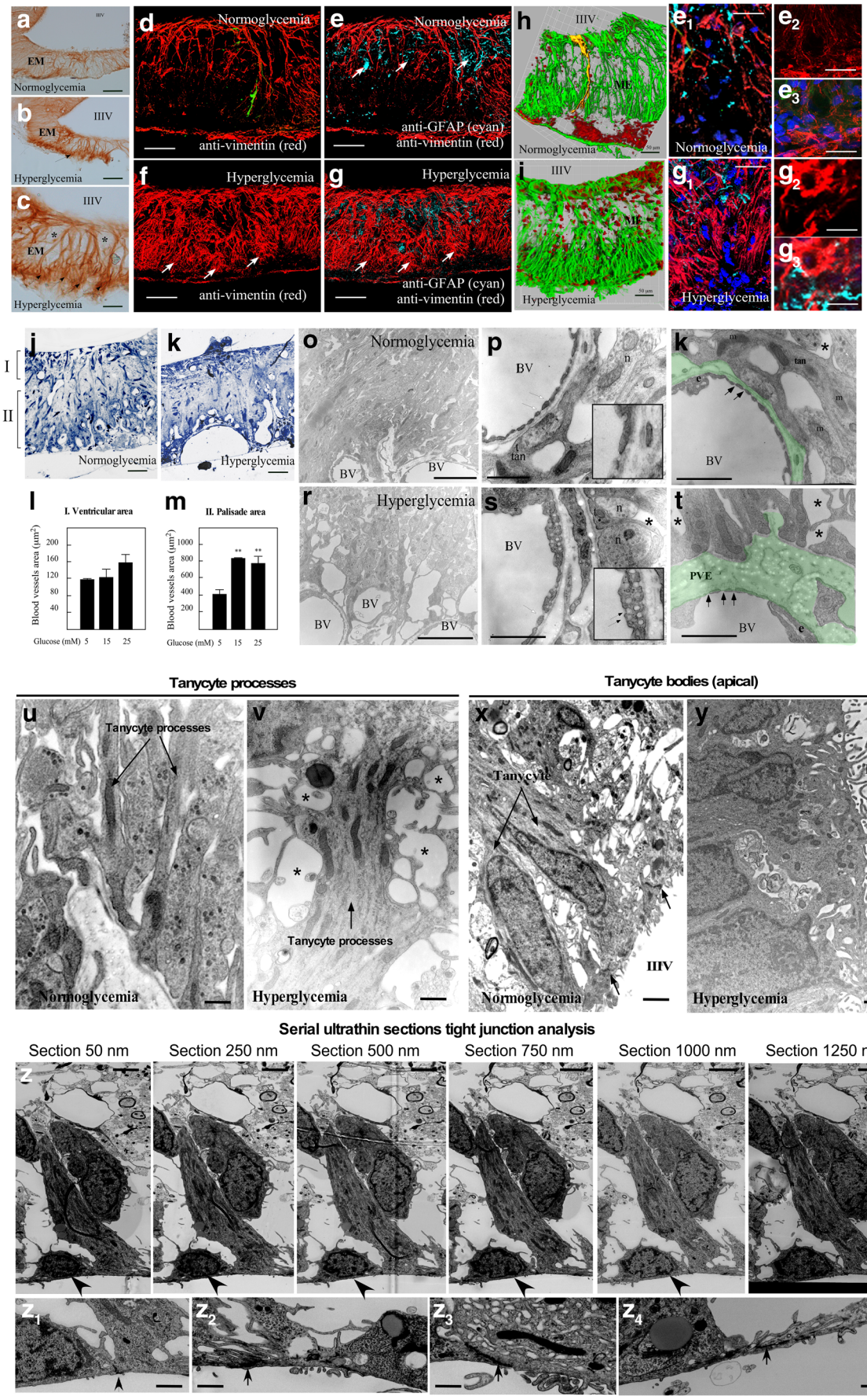

Q2 ◀ **Fig. 3** Analysis of the cellular changes induced by hyperglycemic conditions in tanycytes from the median eminence. **a**–**c** Immunohistochemical analysis of ME tanycytes with anti-vimentin in normoglycemia and hyperglycemia condition. **d**–**g** Confocal analysis and Z-stack/tile imaging of the ME. Analysis with anti-vimentin (red) and anti-GFAP (blue light, arrows) in normo (**d**, **f**) and hyperglycemic (**f**, **g**) condition. The tanycyte branching in the Palisade area is increased in hyperglycemic condition (**f**, **g**, arrows, **e1**–**e3**, and **g1**–**g3**). Nuclear staining with Hoechst in higher magnification pictures. **h**–**i** Confocal analysis and Z-stack of the ME tanycytes and rendering analysis with Imaris software in normo- and hyperglycemic condition. Analysis with anti-vimentin antibodies (green). Nuclear staining in red by using Topro. **j**–**i** Optic and electron microscopy analysis of brain samples processed for the ultrastructural study of blood vessels. Quantitative analysis of ME blood vessels using semi-thin sections staining with toluidine blue in normo- and hyperglycemic condition. Analysis in both ventricular and palisade regions was performed (**j**, **k** and **l**, **m**). Ultrastructural analysis of vascular and perivascular changes induced in hyperglycemic condition (**p**, **q**, **s** and **t**). Perivascular enlargement (PVE) is indicated in green (**t**). Capillary fenestrations are not modified (arrow); however, the endothelial cells changed the number of transcytosis vesicles (**s**, arrows). **u**–**y** Ultrastructural tanycytes processes or bodies (apical) analysis in normo- or hyperglycemic conditions. Tanycytes end-processes enlargement was detected in hyperglycemic condition. Intercellular spaces were also detected forming a "lacunar-like" structures (**v**, asterisk). In the apical area of tanycytes, the subcellular characteristic was similar (**x**, **y**); however, an increase in short microvilli was detected in some part of the ME tanycytes (**y**). **z** and $\mathbf{z_1}$ Ultrastructural serial ultrathin sections to analyze tight junction distribution in 1 μm of tissue thickness. Tight junctions were demarcated with osmium tetroxide treatment ($\mathbf{z_1}$, arrow). Asterisk, inter-tanycytes spaces; BV, blood vessels; n, neurons; tan, tanycytes processes. In **l** and **m**, data are mean ± SD, from 6 animals for experimental condition. $^{**}p < 0.01$; ANOVA with post hoc Tukey. Scale bars: **a**, 100 μm; **b**, 50 μm; **c**, **j**–**k**, 30 μm; **d**–**g**, 50 μm; $\mathbf{e_2}$, $\mathbf{e_3}$, $\mathbf{g_2}$, $\mathbf{g_3}$, 15 μm; $\mathbf{e_1}$, $\mathbf{g_1}$, 25 μm; **o**, **r**, 20 μm; **p**, **s**, 10 μm; **k**, **t**, 5 μm; **u**, **v**, 3 μm; **z**, 6 μm; $\mathbf{z_1}$–$\mathbf{z_4}$, 1 μm. All images are representative of different biologically independent samples. **a**–**c**, $n = 6$ for experimental condition. **d**–**g**, $n = 12$ for experimental condition. **j** and **k**, $n = 6$. **o**, **p**, **k** and **u**, **x**, $n = 6$. **r**, **s**, **t** and **v**, **y**, $n = 6$. **z**, $n = 3$

the glucose concentration reached approximately 18 mM in 5 min, and between 15 and 45 min, the concentration was maintained at approximately 25 mM. At the same time, glycorrhachia increased from approximately 3 to 8 mM in the lateral ventricle, and from approximately 3 to 11 mM in the third ventricle (Fig. 5b). The lateral ventricle never had a glucose concentration higher than that observed in the third ventricle at none of the analyzed times. At the longer time points (30 and 45 min), the difference was significantly greater in the third ventricle, indicating that this cavity is more efficient at increasing glucose concentration in hyperglycemia than the lateral ventricle.

The role of low-affinity transporters in the "fast-track" mechanism was next established in vivo after injecting adenovirus inhibitors for GLUT2 and GLUT6 (AdshGLUT2-GFP or AdshGLUT6-GFP), and evaluating the transfer of glucose to the CSF present in the third ventricle. Adenoviruses injected at the level of the third ventricle showed great efficiency to transduce tanycytes of the ME at 48 h (Supplementary Fig. 2a–k). In addition, the effect generated by GLUT2 and GLUT6 expression in the basal hypothalamus was defined by qRT-PCR. AdshGLUT2-GFP produced an 80% decrease in GLUT2 expression levels without affecting the expression of GLUT6 (Supplementary Fig. 2l). In parallel, transduction with AdshGLUT6-GFP decreases GLUT6 mRNA expression by 50% and GLUT2 expression by 20% (Supplementary Fig. 2m).

Because it was expected that glucose transfer from the ME to the CSF should be very fast, we analyzed the effect generated by the injected adenovirus following inducing hyperglycemia induction for 5 min. In all conditions analyzed, glycemia reached approximately 19 mM by 5 min (Fig. 5c), and the adenovirus injection did not affect this process. However, glycorrhachia of the control animals or injected with Ad siβGal reached 5.9 mM at 5 min, and those injected with Ad siGLUT2 and Ad siGLUT6 reached an approximate glucose concentration of 4.5 mM. These data showed that inhibition of both transporters decreases glucose transfer to the basal third ventricle.

Discussion

Recently, it has been demonstrated that different metabolic conditions alter the structural organization of the blood-hypothalamic barrier, increasing access of metabolic substrates to the arcuate nucleus, a process that is dependent on VEGF signaling (Langlet et al., 2013). Furthermore, it has been shown that leptin is transported through tanycytes of the median eminence to reach mediobasal hypothalamic neurons. This mechanism plays a critical role in the pathophysiology of leptin resistance (Balland et al., 2014) [11]. In the present study, we propose another route of glucose uptake by the CSF through the basal third ventricle, the ME. In this context, it is important to note that the brain has circumventricular organs known as "windows of the brain" [43]. These structures are part of the ventricular walls, and they have fenestrated capillaries that provide high vascular permeability as well as glial cells that come into contact with the blood and the CSF. The high vascular permeability of the circumventricular organs (or part of these) can facilitate the detection of changes in the peripheral glucose concentration because they are directly connected to the blood circulation. With the information currently available, it is possible to conclude that glucose enters the CSF only by the choroid plexus; however, these structures have a low affinity, highly saturable, and fundamentally polarized glucose transporter (GLUT1) in the basolateral membrane. In this way, the amount of glucose transported within the CSF can hardly directly reflect the increase in vascular glucose concentrations.

Our results showed that structural modifications of the tanycytes were observed mainly in the anterior region of the infundibular recess, a phenomenon that was reversible when

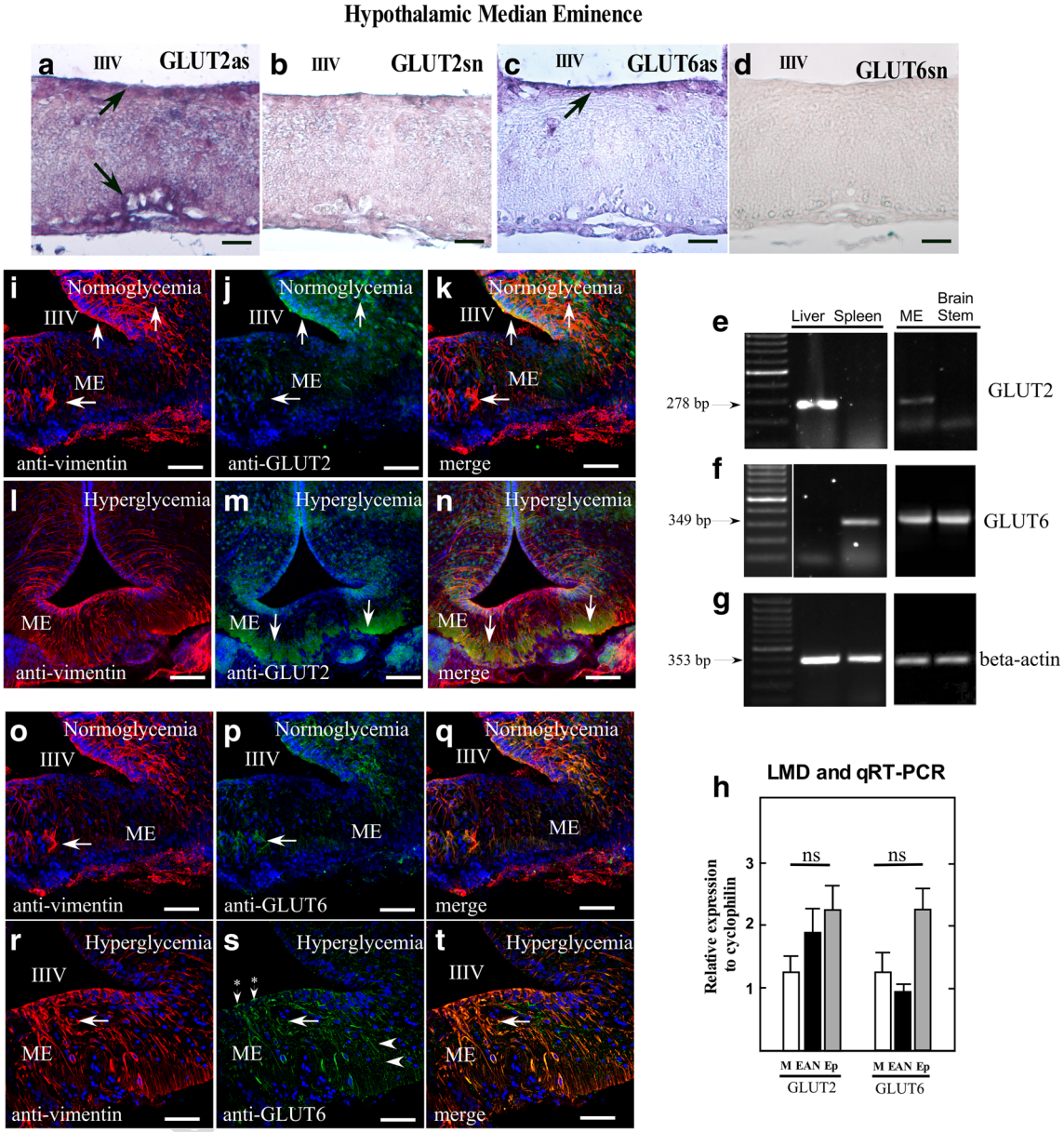

Fig. 4 Increased detection of GLUT2 in end-feet processes contacting fenestrated blood vessels in hyperglycemia with GLUT6 mainly intracellular in median eminence tanycytes. **a**–**d** In situ hybridization of GLUT2 (**a**, **b**) and GLUT6 (**c**, **d**) mRNA in normoglycemia. **e**–**g** RT-PCR analysis of GLUT2 and GLUT6 mRNA expression in the ME and basal hypothalamic area in normoglycemia. **h** Laser microdissection (LMD) comparative analysis of ME tanycytes, arcuate nucleus (AN) area, ependymal cells (ep), and cerebral cortex (cc) to define the relative expression GLUT2 and GLUT6 mRNA. **i**–**n** Confocal microscopy after immunofluorescence analysis to define GLUT2 distribution in normo and hyperglycemic condition. **o**–**t** Confocal microscopy after immunofluorescence analysis to define GLUT6 distribution in normo- and hyperglycemic condition. In **h**, data are mean ± SD, from 4 experimental conditions. ns, not significant; ANOVA with post hoc Tukey. IIIV, third ventricle. Scale bars: **a**–**d**, **i**–**t**, 50 μm. All images are representative of different biologically independent samples. **a**, $n = 6$. **I**–**k**, $n = 6$. **l**–**n**, $n = 6$. **o**–**q**, $n = 6$. **r**–**T**, $n = 6$

recovering normoglycemia. These results are directly connected to the blood circulation of the ME, where the blood flows from the anterior to the posterior regions. In this way, the tanycytes present in the anterior region receive the highest glucose boost before the blood completely fills the portal plexus of the ME [43]. In this scenario, Evans blue was observed in the ME from previous regions to more posterior areas of this structure. The transfer of the dye to the walls of the third ventricle in hyperglycemia was extremely effective, which allows us to postulate a very rapid transfer of Evans blue dye, from β2 tanycytes to β1 and α tanycytes. Strikingly, the dye was detected intracellularly in all types of tanycytes, suggesting that the Evans blue dye can be endocytosed by these cells. Alternatively, intracellular detection may be a technical artifact that must be investigated with different methodologies in future studies. Independent of the transfer

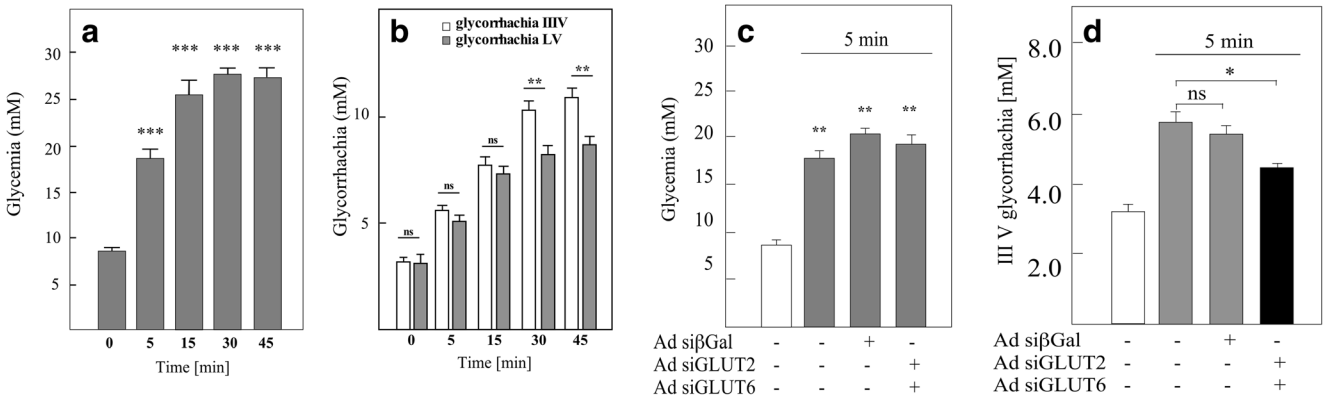

Fig. 5 GLUT2 and GLUT6 inhibition in β2 tanycytes decreased glucose concentration inside the basal third ventricle CSF. **a** Glycemia (mM) analysis was conducted in animals injected intraperitoneally with glucose for 0, 5, 15, 30, and 45 min. **b** Comparative glycorrhachia was analyzed in the CSF of the third ventricle and lateral ventricle in animals injected intraperitoneally with glucose for 0, 5, 15, 30, and 45 min. **c** Glycemia analysis after 5 min of control animals or injected intraperitoneally with glucose after 5 min, after treatment with inhibitor adenovirus Ad siβGal (control), Ad siGLUT2, or Ad siGLUT6. **d** Glycorrhachia analysis after 5 min of control animals or injected intraperitoneally with glucose after 5 min, after treatment with inhibitor adenovirus Ad siβGal (control), or Ad siGLUT2 and Ad siGLUT6. Data are mean ± SD, from 12 (**a**), 9 (**b**), 6 (**c** and **d**) animals for experimental condition. $*p < 0.05$, $**p < 0.01$, $***p < 0.001$; ns, not significant; ANOVA with post hoc Tukey

mechanism, Evans blue reaches the third ventricle and is detected in the ventricular walls of the hypothalamus. We have observed that GLUT2 is expressed and located preferentially in processes that contact the ME capillaries, and GLUT6 is found intracellularly, probably in the ER. Although the mechanism of glucose transfer in β2 tanycytes has not been fully demonstrated in this work, we propose that β2 tanycytes could function as an inverted enterocyte, incorporating glucose of the ME within β2 tanycytes, and then releasing the glucose to CSF using the same GLUT2 transporter localized in the apical membrane [44, 45]. However, GLUT2 was very weakly located at the apical membranes of rat tanycytes. Thus, β2 tanycytes could function in a manner similar to hepatocytes (i.e., glucose phosphorylation to G-6-P followed by incorporation into the ER by G6PT1 [SLC37A4]). Thus, the entry gradient of glucose into the cytosol is favored, and hexokinase 1 inhibition by G-6-P decreases. Within the ER, the molecule is dephosphorylated by glucose-6-phosphatase; thus, glucose may have two routes: (i) glucose can be released from tanycytes by a membrane traffic-based mechanism [46–48] or (ii) glucose can leave the ER again to the cytosol [48]. If this path is feasible, we propose that the glucose transporter for ER output could be GLUT6, a transporter that has di-leucine domains for intracellular retention in the ER. In the cytosol, glucose may be transported to the CSF or could again be phosphorylated to G-6-P, a molecule that activates the glycogen synthetase to store glycogen. Although the routes proposed to secrete glucose within the CSF are biochemically complex, everything aforementioned has been previously observed and demonstrated in liver cells, enterocytes, and recently in astrocytes [46–49].

We have ruled out transit of glucose through ME tight junctions because all electron microscopy analyses showed that tight junctions do not lose their integrity. These data have led us to postulate that GLUT2 and GLUT6 may be involved in the efficient transport of glucose across the ME during hyperglycemia because inhibition of GLUT2 and GLUT6 in β2 tanycytes significantly decreased glucose transfer to the CSF at 5 min. This mechanism could explain why in hyperglycemia, the concentration of glucose in the CSF (basal third ventricle) can reach equal (short time) or higher (long term, 30 min) concentrations as determined in the lateral ventricle of the brain. If glucose diffused to the third ventricle from the lateral ventricle, the glucose concentrations should be very different in both ventricles, especially at very short periods of hyperglycemia (5 min).

The first analysis of GLUT6 location with antibodies in peripheral human tissues was conducted by our research group, confirming some of these results and contributing to the localization of the transporter in the colon, stomach, and distal convoluted tubule kidney [50]. There have also been studies that have evaluated the subcellular distribution of GLUT6, showing its intracellular location, which has been attributed to the presence of di leucine domains similar to that described for GLUT4 [51]. In summary, we postulate that tanycytes rapidly adapt cellular processes that are in contact with the portal vessels in hyperglycemia, increasing the concentration of GLUT2 in their processes. Glucose is captured by tanycytes, a molecule that may be transferred to endomembrane systems. Subsequently, glucose is released to the basal third ventricle CSF by means of exocytosis or glucose transporter functional activity. In periods of fasting, the glucose present in the ER, could enter a futile cycle, leave the ER to the cytosol by means of GLUT6, be phosphorylated to G-6-P, and stimulate the formation of glycogen by means of glycogen synthetase. In this way, the metabolic balance of

tanycytes would be essential to respond to increased glucose concentration at the vascular level.

Materials and methods

Animals

Male Sprague-Dawley rats of 2 months of age were used. The average weight of the adult rats was 275 ± 25 g. The animals were housed in conditions of controlled light (12-h light/dark cycle) and temperature (20–24 °C) and received a standard diet and water ad libitum. The sacrifices were made at the beginning of the light period (9:00–12:00). All procedures were approved by the Bioethics Committee of the Research Department of the University of Concepción.

Induction of normoglycemic and hyperglycemic condition

The 2-month-old rats were fasted for 48 h before glucose injection. Normoglycemia was induced by an intraperitoneal injection of 0.5 g/kg of body weight of glucose to generate a glycemia of 5 mM after 30 min. Hyperglycemia was induced by an intraperitoneal injection of 2 g/kg of body weight of glucose to generate 25 mM blood glucose after 30 min.

Immunohistochemistry, immunofluorescence, and confocal microscopy

For immunohistochemistry, brain frontal slices (40 μm) obtained with vibratome were incubated with hydrogen peroxide at 3% *v/v* in methanol for 30 min to inactivate the endogenous peroxidase and treated using standard methods. For immunofluorescence, the brain tissue was fixed with 4% paraformaldehyde by vascular perfusion. Different sections obtained by freezing microtomy and vibratome were used. For multiple labeling for confocal microscopy, we use antibodies anti-GLUT2 (Alpha Diagnostic Intl. Inc., Texas, USA), anti-GLUT6 (Alpha Diagnostic Intl. Inc.), anti-vimentin (Dako), and anti-glial fibrillary acid protein (GFAP, Dako). As a negative control, the first antibody was omitted. The tissue samples were analyzed by spectral confocal microscopy LSM 780 NLO, Zeiss. Images were acquired with ZEN 2011 software (Zeiss, Germany) after Z-stack and tile-scanning analysis. Imaris software was used for rendering. All observations were made in the antero-medial region of the median eminence considering all the tissue sections around Bregma as working plane − 3.14 (see Supplementary Fig. 1). For optical microscopy with immunoperoxidase or fluorescence analysis, continuous sectioning was performed, and then 1 section of every 5 was selected for analysis. At least 15 sections were analyzed in each middle eminence when the sections were 7 μm. For samples undergoing vibratome sectioning (40 μm) and confocal microscopy analysis, between 6 to 8 sections, were analyzed per animal, covering thickness of approximately 400 μm in width.

Transmission electron microscopy

Sections (90 or 150 μm) fixed in 2% p-formaldehyde and 0.5% glutaraldehyde were rinsed in 0.1 M phosphate buffer and then post-fixed in 2% osmium tetroxide for 1 h. After the sections were rinsed, they were stained with 2% uranyl acetate in 70% ethanol for 3 h, dehydrated in ascending concentrations of alcohol and incubated with propylene oxide for araldite embedding. Once plasticized, the sections were cured at 60 °C for 3 days. Serial semi-thin sections (1.5 μm) were cut in an ultramicrotome (Leica, Wetzlar, Germany) and then stained with 1% toluidine blue. Subsequently, ultrathin (60 nm) sections were cut with a diamond knife using the same ultramicrotome and examined under a Jeol Jem-1400 electronmicroscope. For the generation of 3D ultrastructural data, previously described methods were used [41]. To carry out quantitative analysis in 1-μm sections, the following procedure was performed. At least 20 cuts of 1 μm each were used for the quantification; each cut had a separation of at least 20 μm such that a width of ≥ 200 μm was analyzed.

In situ hybridization

PCR products of GLUT2 (278 bp) and GLUT6 (349 bp) obtained from rat hypothalamic tissue were subcloned into PCR-4-Blunt-TOPO (Clontech, Palo Alto, CA, USA) and used to generate sense and anti-sense digoxigenin-labeled riboprobes. RNA probes were labeled with digoxigenin-UTP by in vitro transcription with SP6 or T7 RNA polymerase following the manufacturer's instructions (Boehringer Mannheim, Mannheim, Germany). In situ hybridization was performed on frontal brain sections mounted on poly-L-lysine-coated glass slides using a previously described method.

Analysis of vascular permeability

Male rats 2 months old were fasted for 48 h to stabilize blood glucose. Subsequently, the normoglycemia and hyperglycemia states were induced for 20 min. After 5 min, the animals were anesthetized with ketamine 90 mg/kg, xylazine 10 mg/kg, and acepromazine maleate 10 mg/kg and a solution of 1% Evans blue was injected through the retro-ocular sinus. The animals were fixed by vascular perfusion with 4% paraformaldehyde and post-fixation by immersion for 48 h. Vibratome slices (40 μm) were used for confocal microscopy analysis.

Adenovirus generation and in vivo inhibition of GLUT2 and GLUT6

Oligonucleotide sequence for GLUT2 (si-rGLUT2-sn1, si-rGLUT2-as1) and GLUT6 (si-rGLUT6-sn1, si-rGLUT6-as1) shRNA, and control oligonucleotide sequence (sense E. coli-βgal; E. coli-βgal anti-sense) were designed, aligned, and then cloned into the vector pDC311.2-OFF-EGFP, which presents a multiple cloning site under the control of the H1 promoter for small RNAs. This vector also encodes the improved green fluorescent protein (EGFP) under the control of the human ubiquitin promoter. The adenoviral particles were produced by recombination of the transfer vectors pDC311.2-GLUT2, pDC311.2-GLUT6, and pDC311.2-βgal with the plasmid pBHGloxDE1,3Cre which has one of the viral genes E1 and E3. Competent adenoviral HEK 293A cells (Invitrogen, Carlsbad, CA, USA) in early passages were seeded at 10^5 cells per well (10 cm^2) in 6-well plates and were co-transfected with pBHGloxΔE1,3Cre vector and transference vectors at a 1:4 M ratio using Lipofectamine 2000 (Invitrogen). Cells were maintained in culture for 10 days with medium replacement (DMEM plus 5% CFS) every 3 days. The detection of a cytopathic effect and the expression of GFP are expected for day 10. In those wells with stronger cytopathic effects, the adenovirus was selected through a cell thermal shock. This viral planting/harvesting protocol was repeated until obtaining an adenovirus titer of 10^9 cfu. The adenovirus titration was performed in HEK 293T cells, observing the expression of the EGFP reporter gene in serial dilutions. A volume of 20 μL was injected into each animal.

Stereotactic methods for glycorrhachia determination

The animals were anesthetized and a cannula guide (PlasticsOne, San Diego, CA, USA) was implanted using the following brain stereotaxic parameters: (i) in lateral ventricle, bregma − 3.14 mm, lateral 4.2 mm, and dorsal-ventral 4.2 mm and (ii) in third basal ventricle, − 3.14 mm, lateral 0.0 mm, and dorsal-ventral 9.2 mm. After 3 days of recovery, we induced normoglycemia and hyperglycemia and the glycorrhachia was determined in CSF isolated from the third ventricle and lateral ventricle. A sample of 2 μL was collected for this procedure and the glucose determinations were performed using Accucheck test strips (Roche Applied Science, Basel, Switzerland). For CSF glucose determination, a factor correction of 1.06 from a calibration curve using artificial CSF was applied. The adenovirus AdshGLUT2-GFP or AdshGLUT6-GFP (20 μL) were injected into the CSF to inhibit GLUT2 and GLUT6 functional expression for 48 h. Ad βGal-GFP was injected as a control.

RT-PCR

Total RNA from the liver, spleen, and media eminence was purified using TRIzol reagent (Invitrogen, Carlsbad, CA, USA) and quantified in a SmartSpec300 spectrophotometer (Bio-Rad, Hercules, CA, USA). For RT-PCR, 1 μg of RNA was pretreated with DNase I (Fermentas, ON, Canada). The basic thermocycling conditions included the following: 1 cycle at 95 °C for 5 min; 35 cycles at 95 °C for 30 s, 60 °C for 30 s, and 72 °C for 30 s; and 1 cycle at 72 °C for 7 min. The following primers were used to analyze the expression of GLUT2 mRNA expression: forward 5′-GGCT AATTTCAGGACTGGTT-3′ and reverse 5′-TTTC TTTGCCCTGACTTCCT-3′ (expected product 278 bp); GLUT6 mRNA expression: GLUT6 forward 5′-TACC TACAGACCATCTTCGACA-3′ and reverse 5′-TCAG ACATGAGGAGCCAGGTGA-3′ (expected product 349 bp); and the housekeeping gene: beta-actin forward 5′-GCTGCTCGTCGACAACGGCTC-3′ and reverse 5′-CAAA CATGATCTGGGTCATCTTCTC-3′ (expected product 349 bp). PCR products were separated by 1.2–1.5% agarose gel electrophoresis and visualized by staining with ethidium bromide.

Laser microdissection and qRT-PCR analysis

Adult rats were sacrificed; the brains were removed and fixed in methacarn (60% methanol, 30% chloroform, and 10% acetic acid) for 3 h at 4 °C. Frontal sections (60 μm) were cut and collected in PBS using a Leica VT1000S vibratome (Leica, Germany) and mounted on polyethylene terephthalate (PET) frame slides (Leica). The different brain areas were dissected with a Leica LMD7000 Laser Microdissector (Leica). Total RNA was extracted with the Ambion RNAqueous-Micro Total RNA Isolation Kit (Ambion, Foster City, CA) following the manufacturer's instructions. For qRT-PCR, standard methods were used and the relative expression of glucose transporters and cyclophilin mRNA was calculated using the $2^{-\Delta\Delta Ct}$ method.

Statistical analysis

All values are expressed as means ± SD. Statistical tests were performed with GraphPad Prism v.7.0a. Unless otherwise noted, for all experiments, where comparisons were made for more than two populations, statistically significance was assessed by one-way or two-way ANOVA with Tukey's multiple comparison post-test. Graphing of data was performed with GraphPad Prism v.7.0a.

Funding information This work was supported by a Fondecyt Iniciación grant 11150678 and a CONICYT PIA ECM-12 grant. The funders had no role in the study.

References

1. Schwartz MW, Woods SC, Porte D Jr, Seeley RJ, Baskin DG (2000) Central nervous system control of food intake. Nature 404(6778):661–671
2. Marty N, Dallaporta M, Foretz M, Emery M, Tarussio D, Bady I, Binnert C, Beermann F, Thorens B (2005) Regulation of glucagon secretion by glucose transporter type 2 (glut2) and astrocyte-dependent glucose sensors. J Clin Invest 115(12):3545–3553
3. Yang XJ, Kow LM, Funabashi T, Mobbs CV (1999) Hypothalamic glucose sensor: similarities to and differences from pancreatic beta-cell mechanisms. Diabetes 48(9):1763–1772
4. Frayling C, Britton R, Dale N (2011) ATP-mediated glucosensing by hypothalamic tanycytes. J Physiol 589 (**Pt 9**:2275–2286
5. Orellana JA, Saez PJ, Cortes-Campos C, Elizondo RJ, Shoji KF, Contreras-Duarte S, Figueroa V, Velarde V, Jiang JX, Nualart F, Saez JC, Garcia MA (2012) Glucose increases intracellular free Ca(2+) in tanycytes via ATP released through connexin 43 hemichannels. Glia 60(1):53–68
6. Garcia M, Millan C, Balmaceda-Aguilera C, Castro T, Pastor P, Montecinos H, Reinicke K, Zuniga F, Vera JC, Onate SA, Nualart F (2003) Hypothalamic ependymal-glial cells express the glucose transporter GLUT2, a protein involved in glucose sensing. J Neurochem 86(3):709–724
7. Maekawa F, Toyoda Y, Torii N, Miwa I, Thompson RC, Foster DL, Tsukahara S, Tsukamura H, Maeda K (2000) Localization of glucokinase-like immunoreactivity in the rat lower brain stem: for possible location of brain glucose-sensing mechanisms. Endocrinology 141(1):375–384
8. Thomzig A, Laube G, Pruss H, Veh RW (2005) Pore-forming subunits of K-ATP channels, Kir6.1 and Kir6.2, display prominent differences in regional and cellular distribution in the rat brain. J Comp Neurol 484(3):313–330
9. Chen R, Wu X, Jiang L, Zhang Y (2017) Single-cell RNA-Seq reveals hypothalamic cell diversity. Cell Rep 18(13):3227–3241
10. Lopez-Gambero AJ, Martinez F, Salazar K, Cifuentes M, Nualart F (2018) Brain glucose-sensing mechanism and energy homeostasis. Mol Neurobiol
11. Prevot V, Dehouck B, Sharif A, Ciofi P, Giacobini P, Clasadonte J (2018) The versatile tanycyte: a hypothalamic integrator of reproduction and energy metabolism. Endocr Rev 39(3):333–368
12. de Vries MG, Arseneau LM, Lawson ME, Beverly JL (2003) Extracellular glucose in rat ventromedial hypothalamus during acute and recurrent hypoglycemia. Diabetes 52(11):2767–2773
13. Shram NF, Netchiporouk LI, Martelet C, Jaffrezic-Renault N, Cespuglio R (1997) Brain glucose: voltammetric determination in normal and hyperglycaemic rats using a glucose microsensor. Neuroreport 8(5):1109–1112
14. Lewis LD, Ljunggren B, Ratcheson RA, Siesjo BK (1974) Cerebral energy state in insulin-induced hypoglycemia, related to blood glucose and to EEG. J Neurochem 23(4):673–679
15. Ono T, Steffens AB, Sasaki K (1983) Influence of peripheral and intracerebroventricular glucose and insulin infusions on peripheral and cerebrospinal fluid glucose and insulin levels. Physiol Behav 30(2):301–306
16. Steffens AB, Scheurink AJ, Luiten PG, Bohus B (1988) Hypothalamic food intake regulating areas are involved in the homeostasis of blood glucose and plasma FFA levels. Physiol Behav 44(4–5):581–589
17. Kurosaki M, Hori T, Takata K, Kawakami H, Hirano H (1995) Immunohistochemical localization of the glucose transporter GLUT1 in choroid plexus papillomas. Noshuyo byori = Brain tumor pathology 12(1):69–73
18. Kumagai AK, Dwyer KJ, Pardridge WM (1994) Differential glycosylation of the GLUT1 glucose transporter in brain capillaries and choroid plexus. Biochim Biophys Acta 1193(1):24–30
19. Rodriguez EM, Gonzalez CB, Delannoy L (1979) Cellular organization of the lateral and postinfundibular regions of the median eminence in the rat. Cell Tissue Res 201(3):377–408
20. Rodriguez EM, Blazquez JL, Guerra M (2010) The design of barriers in the hypothalamus allows the median eminence and the arcuate nucleus to enjoy private milieus: the former opens to the portal blood and the latter to the cerebrospinal fluid. Peptides 31(4):757–776
21. Flament-Durand J, Brion JP (1985) Tanycytes: morphology and functions: a review. Int Rev Cytol 96:121–155
22. Brightman MW, Reese TS (1969) Junctions between intimately apposed cell membranes in the vertebrate brain. J Cell Biol 40(3):648–677
23. Mullier A, Bouret SG, Prevot V, Dehouck B (2010) Differential distribution of tight junction proteins suggests a role for tanycytes in blood-hypothalamus barrier regulation in the adult mouse brain. J Comp Neurol 518(7):943–962
24. Cheunsuang O, Stewart AL, Morris R (2006) Differential uptake of molecules from the circulation and CSF reveals regional and cellular specialisation in CNS detection of homeostatic signals. Cell Tissue Res 325(2):397–402
25. Wright EM, Loo DD, Hirayama BA (2011) Biology of human sodium glucose transporters. Physiol Rev 91(2):733–794
26. Gould GW, Holman GD (1993) The glucose transporter family: structure, function and tissue-specific expression. The Biochemical journal 295(Pt 2):329–341
27. Mueckler M (1994) Facilitative glucose transporters. Eur J Biochem 219(3):713–725
28. McEwen BS, Reagan LP (2004) Glucose transporter expression in the central nervous system: relationship to synaptic function. Eur J Pharmacol 490(1–3):13–24
29. Maher F, Vannucci SJ, Simpson IA (1994) Glucose transporter proteins in brain. FASEB J: Official Publication of the Federation of American Societies for Experimental Biology 8(13):1003–1011
30. Nualart F, Godoy A, Reinicke K (1999) Expression of the hexose transporters GLUT1 and GLUT2 during the early development of the human brain. Brain Res 824(1):97–104
31. Vannucci SJ, Gibbs EM, Simpson IA (1997) Glucose utilization and glucose transporter proteins GLUT-1 and GLUT-3 in brains of diabetic (db/db) mice. Am J Phys 272(2 Pt 1):E267–E274
32. Vannucci SJ, Maher F, Simpson IA (1997) Glucose transporter proteins in brain: delivery of glucose to neurons and glia. Glia 21(1):2–21
33. Brant AM, Jess TJ, Milligan G, Brown CM, Gould GW (1993) Immunological analysis of glucose transporters expressed in different regions of the rat brain and central nervous system. Biochem Biophys Res Commun 192(3):1297–1302
34. Choeiri C, Staines W, Messier C (2002) Immunohistochemical localization and quantification of glucose transporters in the mouse brain. Neuroscience 111(1):19–34
35. Ngarmukos C, Baur EL, Kumagai AK (2001) Co-localization of GLUT1 and GLUT4 in the blood-brain barrier of the rat ventromedial hypothalamus. Brain Res 900(1):1–8
36. Sankar R, Thamotharan S, Shin D, Moley KH, Devaskar SU (2002) Insulin-responsive glucose transporters-GLUT8 and GLUT4 are expressed in the developing mammalian brain. Brain Res Mol Brain Res 107(2):157–165
37. Doege H, Schurmann A, Bahrenberg G, Brauers A, Joost HG (2000) GLUT8, a novel member of the sugar transport facilitator family with glucose transport activity. J Biol Chem 275(21):16275–16280

38. Thorens B (1992) Molecular and cellular physiology of GLUT-2, a high-km facilitated diffusion glucose transporter. Int Rev Cytol 137: 209–238
39. Kellett GL, Helliwell PA (2000) The diffusive component of intestinal glucose absorption is mediated by the glucose-induced recruitment of GLUT2 to the brush-border membrane. The Biochemical journal 350(Pt 1):155–162
40. Doege H, Bocianski A, Joost HG, Schurmann A (2000) Activity and genomic organization of human glucose transporter 9 (GLUT9), a novel member of the family of sugar-transport facilitators predominantly expressed in brain and leucocytes. The Biochemical journal 350(Pt 3):771–776
41. Fiala JC (2005) Reconstruct: a free editor for serial section microscopy. J Microsc 218(Pt 1):52–61
42. Cifuentes M, Baeza V, Arrabal PM, Visser R, Grondona JM, Saldivia N, Martinez F, Nualart F, Salazar K (2018) Expression of a novel ciliary protein, IIIG9, during the differentiation and maturation of ependymal cells. Mol Neurobiol 55(2):1652–1664
43. Duvernoy HM, Risold PY (2007) The circumventricular organs: an atlas of comparative anatomy and vascularization. Brain Res Rev 56(1):119–147
44. Schmitt CC, Aranias T, Viel T, Chateau D, Le Gall M, Waligora-Dupriet AJ, Melchior C, Rouxel O, Kapel N, Gourcerol G, Tavitian B, Lehuen A, Brot-Laroche E, Leturque A, Serradas P, Grosfeld A (2017) Intestinal invalidation of the glucose transporter GLUT2 delays tissue distribution of glucose and reveals an unexpected role in gut homeostasis. Molecular metabolism 6(1):61–72
45. Leturque A, Brot-Laroche E, Le Gall M (2009) GLUT2 mutations, translocation, and receptor function in diet sugar managing. Am J Phys Endocrinol Metab 296(5):E985–E992
46. Stumpel F, Burcelin R, Jungermann K, Thorens B (2001) Normal kinetics of intestinal glucose absorption in the absence of GLUT2: evidence for a transport pathway requiring glucose phosphorylation and transfer into the endoplasmic reticulum. Proc Natl Acad Sci U S A 98(20):11330–11335
47. Guillam MT, Burcelin R, Thorens B (1998) Normal hepatic glucose production in the absence of GLUT2 reveals an alternative pathway for glucose release from hepatocytes. Proc Natl Acad Sci U S A 95(21):12317–12321
48. Burcelin R, del Carmen Munoz M, Guillam MT, Thorens B (2000) Liver hyperplasia and paradoxical regulation of glycogen metabolism and glucose-sensitive gene expression in GLUT2-null hepatocytes. Further evidence for the existence of a membrane-based glucose release pathway. J Biol Chem 275(15):10930–10936
49. Muller MS, Fouyssac M, Taylor CW (2018) Effective glucose uptake by human astrocytes requires its sequestration in the endoplasmic reticulum by glucose-6-phosphatase-beta. Current biology : CB 28(21):3481–3486 e3484
50. Godoy A, Ulloa V, Rodriguez F, Reinicke K, Yanez AJ, Garcia Mde L, Medina RA, Carrasco M, Barberis S, Castro T, Martinez F, Koch X, Vera JC, Poblete MT, Figueroa CD, Peruzzo B, Perez F, Nualart F (2006) Differential subcellular distribution of glucose transporters GLUT1-6 and GLUT9 in human cancer: ultrastructural localization of GLUT1 and GLUT5 in breast tumor tissues. J Cell Physiol 207(3):614–627
51. Lisinski I, Schurmann A, Joost HG, Cushman SW, Al-Hasani H (2001) Targeting of GLUT6 (formerly GLUT9) and GLUT8 in rat adipose cells. The Biochemical journal 358(Pt 2):517–522

AUTHOR QUERIES

AUTHOR PLEASE ANSWER ALL QUERIES.

Q1. Please check if the authors' affiliations are presented/captured correctly.
Q2. Figures 1,3 was not relabeled due to complex data inside the artwork. Please confirm if we can retain the current presentation.
Q3. "Langlet et al., 2013 and Balland et al., 2014" were mentioned here but not in the reference list. Please provide its bibliographic information.
Q4. Please check if the section headings are assigned to appropriate levels.
Q5. The statement "The following primers were used to analyze the expression of GLUT2 mRNA expression: forward 5′-GGCTAATTTCAGGACTGGTT-3′ and reverse...." has been modified. Please check if the intended meaning is retained.
Q6. Reference [42] was provided in the reference list; however, this was not mentioned or cited in the manuscript. As a rule, all references given in the list of references should be cited in the main body. Please provide its citation in the body text.
Q7. Please provide complete bibliographic details of this reference 11.
Q8. [43] has been provided in the reference list but its citation in the text/body is missing. Please advise location of its citation. Otherwise, delete it from the reference list.